

Lower-stratospheric Rossby wave trains in the Southern Hemisphere: A case study for late winter of 1997

By Kazuaki NISHII¹ and Hisashi NAKAMURA^{1,2*}

¹*University of Tokyo, Japan*

²*Institute of Global Change Research, Frontier Research System for Global Change, Japan*

(Received 17 January 2003 ; revised May 2003)

SUMMARY

Behaviour of quasi-stationary circulation anomalies observed in the lower stratosphere of the extratropical Southern Hemisphere during austral late winter of 1997 is studied. The anomalies are defined as daily low-pass-filtered departures from the circulation varying slowly with the seasonal cycle. A wave-activity flux and refractive index for stationary Rossby waves are utilized in our analysis, each of which was defined locally for the zonally varying westerlies. Subseasonal fluctuations in the lower stratosphere were often associated with zonally confined wave trains emanating upward from localized, quasi-stationary anomalies in the troposphere including blocking ridges. The three-dimensional propagation of the waves was found sensitive to the structure of a local waveguide. Upward injection of Rossby wave activity into the stratosphere tended to occur slightly upstream or just beneath of a lower-stratospheric waveguide associated with the developed polar-night jet (PNJ), which led to the subsequent formation of a well-defined wave train downstream along that jet. The distribution of the lower-stratospheric subseasonal variability thus exhibits significant zonal asymmetries, reflecting those in the PNJ structure and the distribution of tropospheric disturbances. Seasonal evolution of the PNJ and that of the tropospheric intraseasonal variability substantially modulated the lower-stratospheric activity of subseasonal fluctuations.

KEYWORDS: Blocking Low-frequency variability Polar-night jet Refractive index Troposphere-stratosphere linkage Wave-activity flux

1. INTRODUCTION

The vertical propagation of planetary waves has been recognized as one of the most fundamental processes involved in the dynamical linkage between the troposphere and stratosphere in the wintertime extratropics. It is now widely accepted that the intensity and meridional-vertical structure of the zonal-mean westerlies significantly influence the vertical propagation of planetary waves from the troposphere to the stratosphere (e.g., Charney and Drazin 1961; Dickinson 1968). Zonal asymmetries in the wintertime stratospheric stationary circulation over the Northern Hemisphere (NH), as observed by Muench (1965) and others, are generated by upward-propagating planetary waves forced by large-scale topography and/or land-sea contrasts (e.g., Matsuno 1970). Temporal variations in the upward propagation are considered to be one of the major causes of the fluctuations observed in the stratospheric circulation. For example, Hirota and Sato (1969) focused the negative correlation between day-to-day variations in the zonal mean westerly wind speed and the amplitude of the zonal wave-number one ($k=1$) component of stratospheric planetary waves. Matsuno (1971) demonstrated that the breakdown of a stratospheric westerly jet during a stratospheric sudden warming event is caused by the planetary waves propagating from the troposphere. Temporal variations in the upward propagating planetary waves have been considered to be caused by various tropospheric processes, including the development of blocking ridges (Julian and Labitzke 1965; Quiroz 1986), the “valving” effect of the tropopause (Chen and Robinson 1992) and the

* Corresponding author: Hisashi Nakamura, Department of Earth and Planetary Science, Graduate School of Science, University of Tokyo, Tokyo, 113-0033 Japan. E-mail: hisashi@eps.s.u-tokyo.ac.jp

nonlinear effect of ensemble of synoptic-scale eddies (Scinocca and Haynes 1998; Hio and Hirota 2002).

It is noteworthy that in most of the previous studies the stratospheric planetary waves have been examined in a particular framework where they are defined as the departure from the zonal mean and then decomposed into the zonal harmonics. In this study, we adopt a different framework in which a quasi-stationary circulation field at a particular instance is decomposed into slow variations associated with the seasonal cycle and deviations from them (i.e., anomalies). The latter component includes submonthly fluctuations associated, for example in the troposphere, with quasi-stationary Rossby wave trains, blocking highs and cut-off lows. Those fluctuations may be localized in the zonal direction in the form of a wave train or wave packet that consists of several centres of action with alternate signs aligning side by side over a particular longitudinal sector. Wavy anomalies in that form cannot be expressed by a single zonal harmonic. Their propagation is likely to be influenced by zonal asymmetries in a slowly varying background flow associated with the seasonal cycle in which they are embedded. Although the particular viewpoint we adopt in this study is rather common in the study of tropospheric variability, there have been only a few applications to the stratospheric circulation. Randel (1988) was the first to depict the zonal and vertical group-velocity propagation of Rossby wave trains with a tropospheric origin in the Southern Hemisphere (SH) stratosphere on the basis of a one-point correlation analysis of geopotential height anomalies. He found the tendency that the upward propagation of the wave trains is more apparent in October than in June. Nakamura and Honda (2002) showed that a zonally-confined wave train in the lower stratosphere over the Eurasian continent originates from the tropospheric anomalies over the North Atlantic that form in association with the late-winter formation of an interannual seesaw in the intensity between the surface Aleutian and Icelandic lows. They found that the location of the lower-stratospheric wave train is in good correspondence to a lower-stratospheric waveguide along the zonally-confined polar-night jet (PNJ).

In this study, we will attempt to extend Randel's (1988) analysis, by examining quasi-stationary fluctuations in the SH upper-tropospheric and lower-stratospheric circulation during austral winter and early spring of 1997. This particular year was characterized by an extraordinarily strong upward flux of Rossby wave activity into the stratosphere (Fig. 1). We will present several pieces of evidence that some Rossby wave trains that developed in the SH lower stratosphere originated from localized quasi-stationary anomalies in the tropospheric circulation including blocking highs. We will show that the characteristics of the three-dimensional group-velocity propagation of those wave trains were substantially modulated by zonal asymmetries in the basic state varying slowly on seasonal time scales. We will argue that behaviour of submonthly, quasi-stationary wavy fluctuations observed in the SH lower stratosphere may be well understood from a particular viewpoint of localized trains of quasi-stationary Rossby waves.

2. DATA AND DIAGNOSTIC METHODS

Our study is based on a reanalysis data set produced jointly by the U. S. National Centers for Environmental Prediction (NCEP) and U. S. National Center for Atmospheric Research (NCAR). The twice daily data of geopotential height, temperature and horizontal wind at 17 pressure levels from 1000 to 10

hPa are used, which are available for 0000 and 1200 UTC on a regular $2.5^\circ \times 2.5^\circ$ latitude-longitude grid. As reported by Trenberth and Stepaniak (2002), the NCEP reanalysis data set has a pathological problem in the stratosphere, which is primarily manifested as a two-grid noise in the vertical direction in the divergent wind field especially above steep topography like the Andes. Yet, this problem would little affect our analysis, because we focus primarily on the SH high latitudes where no apparent erroneous signatures was found in their study.

A digital low-pass filter with a half-power cut-off period of 8 days has been applied to the data time series, in order to extract a quasi-stationary component while eliminating fluctuations associated with migratory, synoptic-scale transient eddies that are strong mainly in the troposphere. Seasonal evolution of the circulation has been obtained in 31-day running mean fields, and the instantaneous deviation of the low-pass-filtered field from the running mean field represents quasi-stationary intraseasonal anomalies. To mimic streamfunction-like anomalies, the geopotential height anomalies have been multiplied by f_0/f , where f is the Coriolis parameter at a given latitude and $f_0 = f(43^\circ\text{S})$.

To represent the three-dimensional propagation of quasi-stationary Rossby wave trains, we utilized a phase-independent wave-activity flux on the log-pressure coordinate formulated by Takaya and Nakamura (1997, 2001). The flux is defined as

$$\mathbf{W} = \frac{p}{2|\mathbf{U}|} \begin{pmatrix} U(v'^2 - \psi'v'_x) + V(-u'v' + \psi'u'_x) \\ U(-u'v' + \psi'u'_x) + V(u'^2 + \psi'u'_y) \\ \frac{f_0 R_a}{N^2 H_0} \{U(v'T' - \psi'T'_x) + V(-u'T' - \psi'T'_y)\} \end{pmatrix}, \quad (1)$$

where ψ' denotes perturbation geostrophic streamfunction, $\mathbf{v}' = (u', v')$ perturbation geostrophic wind velocity, $\mathbf{U} = (U, V)$ a horizontal basic flow velocity, R_a the gas constant of dry air, H_0 the constant scale height, and N the Brunt-Väisälä frequency. The flux is suited for illustrating a “snapshot” of a packet of stationary Rossby waves propagating through the zonally asymmetric westerlies, since in theory, it is independent of wave phase and parallel to the local three-dimensional group velocity vector. In this study, the 31-day running mean field of \mathbf{U} and N is regarded as the basic state in which stationary Rossby waves are embedded and the 8-day low-pass-filtered anomalies of ψ' and \mathbf{v}' are regarded as the wave-associated fluctuations.

In this study, a particular form of the refractive index for stationary Rossby waves introduced by Karoly and Hoskins (1982) on a meridional plane is extended to a zonally asymmetric basic flow as in Karoly (1983). In the log-pressure coordinate, the extended index may be expressed as

$$\kappa_s^2 = \frac{|\nabla_H Q|}{|\mathbf{U}|} - \frac{f_0^2}{4N^2 H_0^2} \left(1 - 4H_0 N \frac{dN^{-1}}{dz} + 4H_0^2 N \frac{d^2 N^{-1}}{dz^2} \right), \quad (2)$$

where Q signifies quasi-geostrophic potential vorticity (PV) of the basic flow and ∇_H the horizontal gradient operator. In our derivation, we apply a WKB-type assumption as adopted by Karoly (1983) and Hoskins and Ambrizzi (1993) in their extension of the refractive index to a zonally varying basic flow on a horizontal plane. See appendix for the derivation of (2). A wave packet tends to be refracted towards the gradient of this index. A band of maxima of the index, if locally defined in the WKB sense, represents a localized waveguide of those waves if the band is associated with a westerly jet, as in an example

given in Nakamura and Honda (2002). The index has been evaluated on the basis of the 31-day running mean fields. Following Chen and Robinson (1992), we neglect the second and third terms in the parentheses in (2) that include derivatives of N^{-1} , in recognition of the fact that vertical variations in N are small except in the immediate vicinity of the discontinuity at the tropopause. A sudden upward increase in N across the tropopause yields negative κ_s^2 locally, which acts to render stationary Rossby waves vertically evanescent or possibly keep those waves trapped around the tropopause. However, the layer of negative κ_s^2 is so thin around the tropopause that the decaying or trapping effect of the layer on planetary waves is generally limited. In the following, each of the κ_s fields thus evaluated has been smoothed zonally by first decomposing the field into the zonal harmonics and then retaining the components of $k \leq 4$. This smoothing is reasonable because only the planetary-wave components can propagate up into the stratosphere and thus only those planetary-scale structure in the mean flow influence the wave propagation.

3. LOWER-STRATOSPHERIC WAVE TRAINS IN OCTOBER 1997

(a) *Development of tropospheric circulation anomalies*

In this section, behaviour of wave trains observed in the SH troposphere and lower stratosphere during October 1997 is investigated. Figure 2 shows the time sequence of low-pass-filtered 400-hPa geopotential height anomalies (ψ') observed in mid-October of 1997. On October 8 (Fig. 2(a)), the tropospheric ψ' field was characterized by a pair of quasi-stationary wave trains, one extending from the South Atlantic into the South Indian Ocean, and the other over the South Pacific sector. While the former wave train was decaying, the latter was developing that consisted of two cyclonic ψ' centres, one to the east of New Zealand (NZ) and the other near the Drake Passage, and of two anticyclonic ψ' centres, one over NZ and the other over the Southeastern (SE) Pacific (marked with a circle). The anticyclonic ψ' over the SE Pacific were developing into a blocking ridge, as in a typical example shown by Renwick and Revell (1999). Our wave-activity flux diagnosis indicates that this blocking amplification was indeed due to the accumulation of wave activity propagating eastward through the Rossby wave train, as shown in Nakamura et al. (1997), Hirasawa et al. (2000) and Swanson (2002). By October 10 (Fig. 2(b)), another cyclonic ψ' centre rapidly developed off Chile in association with a pronounced equatorward flux of wave activity that emanated from the blocking anticyclone over the SE Pacific. With this wave-activity outflow, the anticyclone gradually decayed until it disappeared by October 18 (Fig. 2(f)).

By October 12 (Fig. 2(c)), the other wave train over the Atlantic and Indian Oceans was diminished, except a pair of an anticyclonic ψ' centre over the eastern Indian Ocean and a cyclonic ψ' centre south of Australia (the latter is marked with a square in Fig. 2). As the anticyclonic ψ' developed to the SE of NZ, the two wave trains appeared to be merged together by October 16 (Fig. 2(e)), to form a single wave train that extended from the Indian Ocean to South America. At the same time, another anticyclonic ψ' centre rapidly amplified to the south of Africa, forming a prominent blocking ridge.

(b) *Formation of a lower-stratospheric wave train*

The corresponding time evolution of the lower stratospheric ψ' field observed in the same mid-October period is shown in Fig. 3. Until October 10 (Figs. 3(a) and (b)), only a modest signature of a wave train was noticeable over the Indian Ocean. By October 12 (Fig. 3(c)), a strong anticyclonic ψ' centre developed at the 50-hPa level over the Ross Sea (to the SE of NZ), located slightly downstream of the cyclonic ψ' centre that had amplified in the troposphere (denoted by a square in Figs. 2 and 3). Meanwhile, a strong cyclonic ψ' centre developed in the stratosphere over the Drake Passage, situated slightly downstream of the aforementioned tropospheric blocking ridge (denoted by a circle in Figs. 2 and 3). A strong upward wave-activity flux was observed at the 150-hPa level between these two pairs of the tropospheric and stratospheric ψ' centres. By October 14 (Fig. 3(d)), a weak anticyclonic ψ' centre formed at the 50-hPa level to the south of Africa, followed by the subsequent formation of a weak cyclonic ψ' centre farther downstream ($\sim 70^\circ\text{E}$) by October 16 (Fig. 3(e)). These three ψ' centres seem to form a single wave train in the stratosphere (Fig. 3(e)) that extended along the PNJ from the South Atlantic into the South Indian Ocean. Over this longitudinal sector, the PNJ was the stronger than any other sectors in the presence of the weak $k=1$ component of planetary waves (Fig. 4(c)). Indeed, the associated 50-hPa wave-activity flux was dominantly eastward and mostly confined along the PNJ. This horizontal wave train is reinforced by the weak injection of wave activity from the underlying tropospheric ψ' centre over the Southwestern (SW) Indian Ocean (Figs. 3(e) and (f)). In contrast, the wave-activity flux emanating horizontally from the stratospheric anticyclonic ψ' over the Ross Sea exhibits no apparent downstream spread, despite the pronounced divergence of the flux out of that ψ' centre.

Another insight into the aforementioned troposphere-stratosphere linkage is given in zonal cross-sections for 55°S of low-pass-filtered ψ' and the associated wave-activity flux plotted daily for the mid-October period (Fig. 5). A westward phase tilt with height is obvious between the stratospheric ψ' centres and tropospheric ψ' centres located upstream. The phase tilt is particularly distinct in a layer between the 50 and 100-hPa levels within two longitudinal sectors, one between 120°W and 60°W and the other between 120°E and 180° . The westward phase tilt is consistent with the upward flux of wave activity associated with stationary Rossby wave trains as shown in Figs. 2 and 3.

(c) *Zonally asymmetric waveguide structure*

The basic-state structure for the corresponding period is revealed in a zonal cross-section for 55°S of U and refractive index (κ_s) for stationary Rossby waves averaged over the 31-day period centred on October 12 (Fig. 6). In the lower stratosphere, κ_s is particularly large in the two longitudinal sectors, one over the South Atlantic and SW Indian Oceans ($60^\circ\text{W} \sim 90^\circ\text{E}$) and the other over the South Pacific (around the dateline). Apparently, the former waveguide with larger κ_s associated with the stratospheric PNJ is much better organized and deeper than the latter waveguide that is associated with the tropospheric subpolar jet (SPJ) and confined mainly below the 100-hPa level (Fig. 4(a) and (b)).

As indicated in Figs. 2 and 3, upward injection of wave activity into the stratosphere was particularly strong in the following three longitudinal sectors. Two of them were situated below the PNJ and another over the South Pacific,

each of which was just beneath or slightly upstream of a local lower-stratospheric maximum of κ_s . In fact, the observed wave-activity flux was pointing toward the local maxima of κ_s , which is consistent with the ray tracing theory as explained in Karoly and Hoskins (1982). For example, the strong upward emanation of wave activity from a blocking ridge over the SE Pacific led to the formation of a well-defined wave train downstream in the lower stratosphere (Fig. 5(c)), as the wave-activity emanation occurred at the entrance of the waveguide along the PNJ (Figs. 6 and 7(b)). The subsequent upward injection of wave activity from another blocking ridge south of Africa occurred near the exit of the waveguide (Figs. 5(e), 5(f), and 6), reinforcing the lower-stratospheric wave train (Figs. 3(e) and (f)). In contrast, another event of upward wave-activity emanation from the tropospheric cyclonic ψ' to the south of Australia did not lead to the formation of a horizontal wave train downstream in the stratosphere, since the wave-activity injection occurred just upstream of a well-defined κ_s minimum (Figs. 2(c), 3(e), 6 and 7(b)). Rather, the injected wave activity led to the formation of anticyclonic ψ' isolated within a zonally-confined region of maximum κ_s . Our analysis strongly suggests that not only the meridional and vertical configurations but also the zonal configuration of the lower-stratospheric time-mean westerlies is a crucial factor for determining the formation and propagation of a wave train in the lower stratosphere.

4. SEASONALITY IN THE THREE-DIMENSIONAL WAVE PROPAGATION

In this section, localities of three-dimensional wave-activity propagation and its seasonal dependence are discussed in relation to the seasonal evolution in the three-dimensional waveguide structure. Figure 8 shows maps of 400-hPa time-mean U (left column) and the standard deviation of quasi-stationary ψ' (hereafter referred to as $\sigma(\psi')$) at the 400-hPa level for each of the four 31-day periods as indicated, superimposed on the associated local wave-activity flux averaged over the corresponding period (right column). The four periods are centred at the first days of July (a,b), August(c,d), September(e,f) and October (g,h), hereafter referred to as Periods I, II, III and IV, respectively. Period IV ended before the final stratospheric warming that began in late October associated with changes in U (Fig. 1(c)). The breakdown of the WKB-type approximation would have occurred if the October-mean field had been used in our wave-activity diagnosis.

In each of the four periods, the strength of tropospheric submonthly fluctuations, as measured by 400-hPa $\sigma(\psi')$, was distributed in a zonally asymmetric manner (Figs. 8(b), (d), (f) and (h)). The upper-tropospheric $\sigma(\psi')$ remained strong in all of the four periods around the exit region of the SPJ over the South Pacific, including the region of frequent blocking formation south of NZ (Renwick and Revell 1999), and also around the entrance of that jet over the SE Atlantic and SW Indian Oceans. The wave activity propagated mostly eastward along the SPJ (at $50^\circ \sim 60^\circ\text{S}$) out of those regions of maximum $\sigma(\psi')$. The tropospheric $\sigma(\psi')$ tended to be strong also around the exit of the subtropical jet off Chile and over Argentina. The mean horizontal wave-activity flux was divergent out of these regions, with an apparent equatorward component especially over the SW Atlantic. The upward injection of wave activity into the stratosphere occurred mainly in those regions of the enhanced tropospheric fluctuations located beneath the prominent stratospheric PNJ during late winter and early spring (Figs. 8(d), (f) and (h)).

Among the four periods for our analysis, the wave-activity injection into the stratosphere was weakest in Period I (16 June \sim 16 July), despite the fact that tropospheric $\sigma(\psi')$ was nearly as strong as in the three other periods (Fig. 8(b)). As evident in Fig. 1(c), the upward injection was suddenly enhanced in late July, which can be related to the seasonal evolution of the waveguide structure associated with the lower-stratospheric PNJ (Figs. 9(a), (b), (d) and (e)). Among those four periods, the lower-stratospheric waveguide was least organized in Period I, particularly around the 100-hPa level. In that period, the PNJ at the 100- and 50-hPa levels is weaker and meridionally less sharp than in any other periods (Figs. 9(a) and 10(a)). The tropospheric fluctuations were most enhanced over the SE Pacific, where the subpolar waveguide at the 100-hPa level was least organized along the SPJ and therefore unfavorable for wave-activity propagation into the stratosphere (Figs. 9(a-c)). In fact, no region of $\kappa_s > 3$ was found below the 70-hPa level over the SE Pacific, as evident in a meridional section of κ_s and U averaged zonally between 60°W and 120°W (Fig. 9(c)). As the stratospheric PNJ matured in Periods II and III, a well-defined waveguide formed near the bottom of the stratosphere underneath the PNJ core (Figs. 9(e), (h) and (k)). In the SE Pacific sector, a band of well-defined maxima of κ_s extended below the PNJ core down to the tropopause level (Figs. 9(f) and (i)). It is this deep waveguide below the PNJ core through which the upward wave-activity propagation into the stratosphere occurred over the SE Pacific in Periods II and III. The only exception was the profound upward flux observed in Period II to the south of NZ, where the 100-hPa κ_s did not exhibit a well-defined local maximum (Fig. 9(e)). Presumably, the wave-activity injected from the troposphere was strong enough to reach into the lower-stratospheric PNJ, despite the lack of a well-organized local waveguide. The aforementioned change in the lower-stratospheric waveguide structure that occurred in July may be associated with the poleward and downward shift of the PNJ core, as shown by Shiotani and Hirota (1985). The shift, however, cannot be confirmed in our study, due to the lack of upper-stratospheric data in the NCEP/NCAR reanalyses. In Period IV, the PNJ started to decay and so did the associated vertical waveguide structure, particularly over the SE Pacific (Figs. 9(j-l)), which is in good agreement of the weakening of the upward wave-activity propagation observed in the particular longitudinal sector (Fig. 8(h)). Nevertheless, the upward wave-activity propagation remained strong over the South Atlantic and Indian Oceans (Fig. 9(k)), where tropospheric $\sigma(\psi')$ was strongest in Period IV (Fig. 8(h)) and the PNJ core was overlapped with the SPJ (Fig. 8(j) and 9(j)) to form a well-defined vertical waveguide (Fig. 9(k)).

It is evident in Fig. 10 that local magnitude of 50-hPa $\sigma(\psi')$ was substantially modulated in corresponding to the wave-activity injection from the troposphere, which was found sensitive to the local waveguide structure as discussed above. At the 50-hPa level, the submonthly ψ' fluctuations were strongly suppressed in Period I, as consistent with the suppressed cross-tropopause wave-activity injection (Fig. 10(c)) under the prematured PNJ (Fig. 10(a)). The fluctuations were drastically enhanced after mid-July, as the wave-activity injection from the troposphere was also enhanced (Figs. 10(f) and (i)) through the well-defined vertical waveguide under the matured PNJ (Figs. 10(d) and (g)). A slight weakening of $\sigma(\psi')$ over the South Pacific in Period IV is consistent with the reduced upward wave-activity injection in that region from the troposphere associated with the breakdown of the local waveguide. It is also evident in Fig. 10 that 50-hPa $\sigma(\psi')$ and the associated horizontal wave-activity flux at

the 50-hPa level both exhibited a certain degree of zonal asymmetry, while confined meridionally in and around the local maxima of κ_s along the PNJ. The zonal asymmetries were particularly apparent in the $\sigma(\psi')$ distribution, which was more asymmetric in the zonal direction than the distribution of U . Local maxima of $\sigma(\psi')$ in the lower stratosphere tended to be located over or slightly downstream of the regions where marked wave-activity injection occurred from the troposphere. At the 50-hPa level, the mean wave-activity flux tended to diverge out of those regions downstream along the PNJ. These results strongly suggest the presence of localized wave trains in the lower stratosphere originated from localized tropospheric circulation anomalies, which cannot be resolved in a straightforward manner within the conventional framework based on the zonal harmonic decomposition.

5. DISCUSSION

It has been shown in many of the previous studies and also obvious in our analysis that the $k=1$ planetary-wave component contributed substantially to the observed circulation anomalies associated with lower-stratospheric wavy anomalies. The waves are embedded in the PNJ whose localization is also due to the steady $k=1$ component in the time-mean flow. This situation may lead to the breakdown of the WKB-type assumption of weak zonal asymmetries in a basic flow adopted in the derivation of a wave-activity flux of Takaya and Nakamura (1997, 2001) and also in the local evaluation of κ_s in our study. Thus, application of these two diagnostic methods to this particular situation cannot be formally justified *a priori*. It is therefore necessary to assess the *qualitative* validity of the WKB-type assumption *a posteriori*. The good correspondence shown in our study between the distribution of the particular wave-activity flux and localized waveguides as defined on the basis of local κ_s suggests that the assumption was *qualitatively* valid for the particular analysis period. At the same time, their good correspondence also suggests the importance of zonal asymmetries in the time-mean flow to the formation and propagation of Rossby wave trains even in the lower stratosphere, which was not considered in the analysis of Randel (1988). In his study, statistics for all the reference grid points along a given latitudinal circle were combined into a one-point correlation analysis. Of course, our framework has limitation. For example, it cannot be applied to an analysis of stratospheric sudden warming during which the background westerlies change dramatically.

Next, it may be instructive to compare our framework with the conventional one in the analysis of the lower-stratospheric circulation anomalies observed during our analysis period. The low-pass-filtered 50-hPa ψ' at 55°S was quasi-stationary in the Eulerian sense, but they tended to exhibit slow and rather regular eastward phase migration (Fig. 11(a)). This phase migration was interrupted rather frequently by the formation of strong stationary anomalies in association with the enhanced upward wave-activity injection from the troposphere. The formation was immediately followed by the downstream development of another anomaly with the opposite sign. This is a signature of the formation of a wave train in the lower stratosphere, which was always associated with a prominent eastward wave-activity flux. It is evident in Fig. 11(b) that the $k=1$ component of the planetary waves as a whole, including their climatological mean component, tend to amplify with the formulation of those wave trains with a tropospheric origin, especially during August and September. In each of the amplification

events in these two months, the slow phase migration of the $k=1$ component was halted temporarily. The $k=2$ component exhibits more pronounced eastward phase migration (Fig. 11(c)), which is presumably a manifestation of the eastward travelling $k=2$ waves in the SH stratosphere with the period of about 2 weeks (Harwood 1975; Hartmann 1976). This regular phase migration also tended to slow down slightly during the formation of the wave packets. Though somewhat masked by the phase migration signatures, the $k=2$ component also amplified in those events of the wave-train formation as the $k=1$ component did (Fig. 11(c)). The aforementioned correspondence between the formation of wave trains in the lower stratosphere and the amplification of the two planetary-wave components can be confirmed in Fig. 12, in which time series of the zonally-averaged flux components associated with submonthly fluctuations and the amplitudes of the $k=1$ and $k=2$ components are plotted. It should be remembered that not only the horizontal heat flux associated with subseasonal fluctuations in the form of zonally-confined wave trains but also the heat flux associated with the climatological-mean planetary waves and their interaction with the submonthly fluctuations were incorporated into the instantaneous upward propagation of the $k=1$ and $k=2$ components. It is hence understandable that the strength of the upward wave-activity flux associated with the wave trains and the amplitude of each of the $k=1$ and $k=2$ planetary-wave components were not well correlated. Nevertheless, it is noteworthy that almost all the events of the augmented upward wave-activity injection associated with the wave trains corresponded to subseasonal amplification events of the $k=1$ and/or $k=2$ components (Fig. 12). It is therefore suggested that the upward propagation of a Rossby wave train with a tropospheric origin is likely to contribute to the subseasonal modulation in the planetary-wave field over the extratropical SH when a well-defined waveguide forms in the course of the seasonal development of the PNJ[†]

In the rest of this section, we will present a caveat in discussing the dynamical linkage between the troposphere and stratosphere based on zonally-averaged statistics as in the conventional framework. We evaluated the refractive index for stationary Rossby waves ($\bar{\kappa}_s$) based on the zonally-averaged zonal westerlies (\bar{U}) and static stability separately for Periods I (Fig.13(a)) and II (Fig.13(c)). Wave-activity propagation in the meridional plane was expressed by means of the conventional Eliassen-Palm (E-P) flux (\mathbf{F}) (Andrews and McIntyre 1976), which is defined for submonthly fluctuations as

$$\mathbf{F} = p \left(\begin{array}{c} -\overline{[u'_* v'_*]} \\ \frac{f_0 R_a}{HN^2} \overline{[v'_* T'_*]} \end{array} \right), \quad (3)$$

where $[]$ denotes zonal averaging, $()_*$ a deviation from the zonal mean, and other notations are the same as in (1). This flux is considered to be associated with submonthly fluctuations, whose zonally-averaged magnitude defined as $Z_s = \sqrt{\overline{[z'^2]}}$, was shown in the meridional sections in Figs. 13(b) and (d) for Periods I and II, respectively. A zonally-averaged vertical waveguide appeared to be well defined in the lower stratosphere in each of the two periods, although the PNJ was somewhat stronger in Period II than in Period I. The zonally-averaged activity of the submonthly fluctuations in the upper troposphere were comparably

[†] An alternative description might be that variations in the lower-stratospheric $k=1$ component extended downward into the upper troposphere, leading to zonal variations in the westerlies. This $k=1$ anomaly pattern interacted with $k=2$ component leading to enhanced $k=2$ activity.

strong along the SPJ in the two periods, although they were slightly stronger in Period II than in Period I (Figs. 13(b) and (d)). In Period I, however, activity of the submonthly fluctuations decayed upward faster than in Period II. In fact, the lower-stratospheric $\sigma(\psi')$ in Period I was nearly half of that in Period II, which is attributable to substantially weaker upward \mathbf{F} in the lower stratosphere associated with the submonthly fluctuations in Period I than in Period II. The weakness of \mathbf{F} in Period I is apparently inconsistent with the well-defined waveguide structure that emerged in the zonally-averaged picture (Fig. 13). As discussed in the previous section, a vertical waveguide had not yet matured in Period I over the regions of the active upper-tropospheric fluctuations including the SE Pacific, while a lower-stratospheric waveguide was formed in Period I along the PNJ over the SE Atlantic, South Indian Ocean and SW Pacific, where the submonthly fluctuations were weak in the troposphere. It is thus suggested that for Period I the observed “mismatch” between the strong tropospheric variability over the western Hemisphere and the well-defined vertical waveguide over the eastern Hemisphere is blurred in the zonally-averaged statistics, yielding the apparent inconsistency among the vertical profiles of $\bar{\kappa}_s$, \bar{U} , \mathbf{F} and Z_s . A comparison between Fig. 13 and a set of Figs. 8, 9 and 10 strongly suggests that the zonal asymmetries in the waveguide structure and wave propagation must be taken into account in discussing the dynamical linkage between the troposphere and lower stratosphere even in the SH.

6. CONCLUDING REMARKS

In this study, the origin and behaviour of quasi-stationary Rossby wave trains observed in the lower stratosphere of the extratropical SH during late winter of 1997 have been analyzed. In section 3, we analyzed in detail a particular event observed in mid-October, as a typical example of the formation of a lower-stratospheric wave train with a tropospheric origin. In section 4, we extended our analysis to the entire winter and early spring of the year, to generalize our findings in the mid-October event.

Several pieces of evidence have been presented to show that submonthly fluctuations in the lower stratosphere were often associated with localized wave trains propagating upward from strong localized quasi-stationary anomalies in the troposphere including blocking highs. Three-dimensional propagation of the wave trains was found sensitive to the three-dimensional structure of a waveguide that could allow wave activity to propagate upward from the tropospheric anomalies into the lower stratosphere and then downstream. Specifically, the strength and sharpness of the stratospheric PNJ and its overlapping with the tropospheric SPJ were found crucial in determining the waveguide structure. The position of developing tropospheric anomalies relative to the PNJ was also found crucial for the effectiveness of wave-activity injection into the stratosphere. It is suggested that our framework with a notion of a “zonally-confined wave train” propagating through the zonally-varying westerlies may give another insight into submonthly modulations in the lower-stratospheric planetary waves, which used to be interpreted from a view point of the interaction between the $k=1$ and $k=2$ planetary components (e.g., Shiotani et al 1990; Hirota and et al 1990; Ushimaru and Tanaka 1992). We have presented a case where the conventional view based on zonally averaged statistics and diagnoses can lead to a misleading interpretation of the observed troposphere and stratosphere dynamical linkage.

ACKNOWLEDGEMENTS

The authors are grateful to Drs. H. Niino and K. Takaya for their valuable comments and advice during the course of this study. They also thank Dr. N. Hirasawa for his comment on Antarctic blocking highs. The authors' thanks are extended to Professors D. J. Karoly and I. Hirota and an anonymous referee for their careful reading of the earlier version of the manuscript and giving us sound criticism and a number of useful suggestions. The Grid Analysis and Display System (GrADS) was used for drawing the figures.

APPENDIX

Derivation of the local refractive index of stationary Rossby waves on the zonally varying westerlies

We begin with the unforced, quasi-stationary potential vorticity (PV) equation in the log-pressure coordinate:

$$\frac{\partial q}{\partial t} + u \frac{\partial q}{\partial x} + v \frac{\partial q}{\partial y} = 0, \quad (\text{A.1})$$

where $(u, v)^T = \mathbf{u} = (-\psi_y, \psi_x)^T$ is the geostrophic velocity. On a β plane, PV is defined as:

$$q = f_0 + \beta y + \frac{\partial^2 \psi}{\partial x^2} + \frac{\partial^2 \psi}{\partial y^2} + \frac{f_0^2}{p} \frac{\partial}{\partial z} \left(\frac{p}{N^2} \frac{\partial \psi}{\partial z} \right). \quad (\text{A.2})$$

We consider small-amplitude perturbations embedded in a steady, zonally inhomogeneous flow $\mathbf{U} = (U, V, 0)^T$, which allows us to represent the variables as:

$$u = U(x, y, z) + u'; \quad v = V(x, y, z) + v'; \quad \psi = \Psi(x, y, z) + \psi'; \quad q = Q(x, y, z) + q'; \quad (\text{A.3})$$

where perturbations are denoted by primes. Then (A.1) may be linearized as:

$$\frac{\partial q'}{\partial t} + \mathbf{U} \cdot \nabla_H q' + \mathbf{u}' \cdot \nabla_H Q = 0, \quad (\text{A.4})$$

where

$$q' = \frac{\partial^2 \psi'}{\partial x^2} + \frac{\partial^2 \psi'}{\partial y^2} + \frac{f_0^2}{p} \frac{\partial}{\partial z} \left(\frac{p}{N^2} \frac{\partial \psi'}{\partial z} \right) \quad (\text{A.5})$$

and ∇_H is the horizontal gradient operator. Here, we adopt what may be called a ‘‘local coordinate rotation’’ technique as in an appendix of Takaya and Nakamura (2001), with which (A.4) is converted onto the local X - Y coordinate system with the X -axis taken in the direction of \mathbf{U} and the Y -axis perpendicular to it (poleward if $Y > 0$) at a particular location. It follows that,

$$\frac{\partial q'}{\partial t} - \frac{\partial \Psi}{\partial Y} \frac{\partial q'}{\partial X} + \frac{\partial Q}{\partial Y} \frac{\partial \psi'}{\partial X} - \frac{\partial Q}{\partial X} \frac{\partial \psi'}{\partial Y} = 0. \quad (\text{A.6})$$

Under the assumption that a steady basic flow is nearly unforced, i.e., $\mathbf{U} \cdot \nabla_H Q \approx 0$, (A.6) becomes,

$$\frac{\partial q'}{\partial t} + U \frac{\partial q'}{\partial X} + \frac{\partial Q}{\partial Y} \frac{\partial \psi'}{\partial X} = 0. \quad (\text{A.7})$$

Scaling the perturbation stream function in (A.5) as $\chi' = p^{\frac{1}{2}}\psi'/N$ yields

$$q' = \frac{N}{p^{\frac{1}{2}}} \left(\frac{\partial^2}{\partial X^2} + \frac{\partial^2}{\partial Y^2} - \alpha^2 n^2 + \alpha^2 \frac{\partial^2}{\partial z^2} \right) \chi', \quad (\text{A.8})$$

where

$$n^2 \equiv \frac{1}{4H^2} \left(1 - 4HN \frac{dN^{-1}}{dz} + 4H^2 N \frac{d^2 N^{-1}}{dz^2} \right),$$

and H is scale height ($z = -H \ln p$) and $\alpha^2 \equiv f_0^2/N^2$ under the assumption that p and N are slowly varying on the horizontal plane. Provided that Ψ and Q are slowly varying function in space, the dispersion equation for plane-wave solutions of (A.7) in the form of

$$\chi' = \chi_0 \exp i(KX + LY + mz - \omega t), \quad (\text{A.9})$$

may be given as

$$\omega = UK - \frac{|\nabla_H Q|K}{K^2 + L^2 + \alpha^2(m^2 + n^2)}, \quad (\text{A.10})$$

where K and L are the locally-defined wave-numbers of the X and Y directions, respectively, and $\partial Q/\partial Y = |\nabla_H Q|$ for the unforced basic flow. This relation is equivalent to Eq. (9) of Karoly and Hoskins (1982). The ‘‘total wave-number’’ is defined locally as $\kappa = (K^2 + L^2 + \alpha^2 m^2)^{\frac{1}{2}}$, which may be expressed in terms of the basic-state quantities as

$$\kappa^2 = \frac{|\nabla_H Q|}{|U| - C_p} - \alpha^2 n^2, \quad (\text{A.11})$$

where C_p is the phase speed in the direction of basic flow, and $C_p = 0$ for stationary Rossby waves. In this coordinate system, the medium is locally homogeneous in the X direction. One can hence consider K to be approximately constant along a wave ray, and a wave packet is inclined to be refracted toward the direction of $\nabla \kappa$, as argued in Karoly and Hoskins (1982) for a zonally uniform basic state. A region of maximum κ (with $C_p = 0$) potentially acts as a waveguide for quasi-stationary Rossby waves in the zonally inhomogeneous westerlies.

REFERENCES

- | | | |
|---------------------------------------|------|---|
| Andrews, D. G. and
McIntyre, M. E. | 1976 | Planetary waves in horizontal and vertical shear: The generalized Eliassen-Palm relation and the mean zonal acceleration. <i>J. Atmos. Sci.</i> , 33 , 2031–2048 |
| Charney, J. G. and Drazin, P. G. | 1961 | Propagation of planetary-scale disturbances from the lower into the upper atmosphere. <i>J. Geophys. Res.</i> , 66 , 83–110 |
| Chen, P., and Robinson, W. A. | 1992 | Propagation of planetary waves between the troposphere and stratosphere. <i>J. Atmos. Sci.</i> , 49 , 2533–2545 |
| Dickinson, R. E. | 1968 | Planetary Rossby waves propagating vertically through weak westerly wind wave guides. <i>J. Atmos. Sci.</i> , 25 , 984–1002 |
| Hartmann, D. L. | 1976 | The structure of the stratosphere in the Southern Hemisphere during late winter 1973 as observed by satellite. <i>J. Atmos. Sci.</i> , 33 , 1141–1154 |
| Harwood, R. S. | 1975 | The temperature structure of the Southern Hemisphere stratosphere August-October 1971. <i>Q. J. R. Meteorol. Soc.</i> , 101 , 75–91 |
| Hio, Y. and Hirota, I. | 2002 | Interannual variations of planetary waves in the Southern Hemisphere stratosphere. <i>J. Meteor. Soc. Japan.</i> , 80 , 1013–1027 |

- Hirasawa, N., Nakamura, H. and Yamanouchi, T. 2000 Abrupt changes in meteorological conditions observed at and inland Antarctic station in association with wintertime blocking. *Geophys. Res. Lett.*, **27**, 1911–1914
- Hirota, I. and Sato, Y. 1969 Periodic variation of the winter stratospheric circulation and intermittent vertical propagation of planetary waves. *J. Met. Soc. Japan*, **47**, 390–402
- Hirota, I., Kuroi, K. and Shiotani, M. 1990 Midwinter warmings in the Southern-Hemisphere stratosphere in 1988. *Q. J. R. Meteorol. Soc.*, **116**, 929–941
- Hoskins, B. J. and Ambrizzi, T. 1993 Rossby wave propagation on a realistic longitudinally varying flow. *J. Atmos. Sci.*, **50**, 1661–1671
- Julian, P. R. and Labitzke, K. B. 1965 A study of atmospheric energetics during the January–February 1963. *J. Atmos. Sci.*, **22**, 597–610
- Karoly, D. J. and Hoskins, B. J. 1982 Three dimensional propagation of planetary waves. *J. Meteor. Soc. Japan*, **60**, 109–123
- Karoly, D. J. 1983 Rossby wave propagation in a barotropic atmosphere. *Dyn. Atmos. Oceans*, **7**, 111–125
- Kalnary, M. E., Kanamitsu, M., Kistler, R., Collins, W., Deaven, D., Gandin, L., Iredell, M., Saha, S., White, G., Woollen, J., Zhu, Y., Leetmaa, A., Reynolds, R., Chelliah, M., Ebisuzaki, W., Higgins, W., Janowiak, J., Mo, K. C., Ropelewski, W., Wang, J., Jenne, R. and Joseph, D. 1996 The NCEP/NCAR 40-year reanalysis project. *Bull. Amer. Meteor. Soc.*, **77**, 437–471
- Matsuno, T. 1970 Vertical propagation of stationary planetary waves in the winter Northern Hemisphere. *J. Atmos. Sci.*, **27**, 871–883
- Matsuno, T. 1971 A dynamical model of the stratospheric sudden warming. *J. Atmos. Sci.*, **28**, 1479–1494
- Muench, H. S. 1965 On the dynamics of the wintertime stratosphere circulation. *J. Atmos. Sci.*, **22**, 349–360
- Nakamura, H., Nakamura, M. and Anderson, J. L. 1997 The role of high- and low-frequency dynamics in blocking formation. *Mon. Wea. Rev.*, **125**, 2074–2093
- Nakamura, H. and Honda, M. 2002 Interannual seesaw between the Aleutian and Icelandic lows. Part III: Its influence upon the stratospheric variability. *J. Meteor. Soc. Japan*, **80**, 1051–1067
- Quiroz, R. S. 1986 The association of stratospheric warmings with tropospheric blocking. *J. Geophys. Res.*, **91**, 5277–5285
- Randel, W. J. 1988 The seasonal evolution of planetary waves in the Southern Hemisphere stratosphere and troposphere. *Q. J. R. Meteorol. Soc.*, **114**, 1385–1409
- Renwick, J. A. and Revell, M. J. 1999 Blocking over the South Pacific and Rossby wave propagation. *Mon. Wea. Rev.*, **127**, 2233–2247
- Scinocca, J. F. and Haynes, P. H. 1998 Dynamical forcing of stratospheric planetary waves by tropospheric baroclinic eddies. *J. Geophys. Res.*, **55**, 2361–2392
- Shiotani, M. and Hirota, I. 1985 Planetary wave-mean flow interaction in the stratosphere: A comparison between Northern and Southern Hemispheres. *Q. J. R. Meteorol. Soc.*, **111**, 309–334
- Shiotani, M., Kuroi, K. and Hirota, I. 1990 Eastward traveling waves in the Southern Hemisphere stratosphere during the spring of 1983. *Q. J. R. Meteorol. Soc.*, **116**, 913–927
- Swanson, K. L. 2002 Dynamical aspects of extratropical tropospheric low-frequency variability. *J. Climate*, **15**, 2145–2162
- Takaya, K. and Nakamura, H. 1997 A formulation of a wave-activity flux for stationary Rossby waves on a zonally varying basic flow. *Geophys. Res. Lett.*, **24**, 2985–2988
- Takaya, K. and Nakamura, H. 2001 A formulation of a phase-independent wave-activity flux for stationary and migratory quasi-geostrophic eddies on a zonally-basic flow. *J. Atmos. Sci.*, **58**, 608–627
- Trenberth, K. E. and Stepaniak, D. P. 2002 A pathological problem with NCEP reanalyses in the stratosphere. *J. Climate*, **15**, 690–695

- Ushimaru, S. and Tanaka, H. 1992 A numerical study of the interaction between stationary Rossby waves and eastward-traveling waves in the Southern-Hemisphere stratosphere. *J. Atmos. Sci.*, **49**, 1354–1373

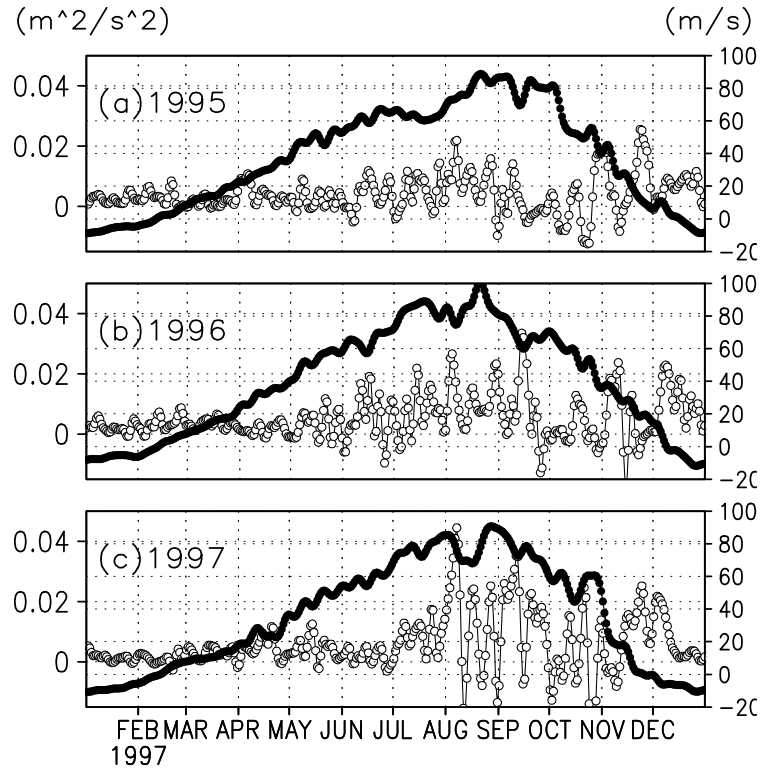


Figure 1. Daily time series of 20-hPa zonal wind speed U (ms^{-1} ; solid line with closed circle; right axis) and the vertical component of a 150-hPa wave-activity flux W_z for stationary Rossby waves (m^2s^{-2} ; open circle; left axis), as defined in section 2. U and W_z have been zonally averaged for 60°S and plotted separately for (a) 1995, (b) 1996 and (c) 1997.

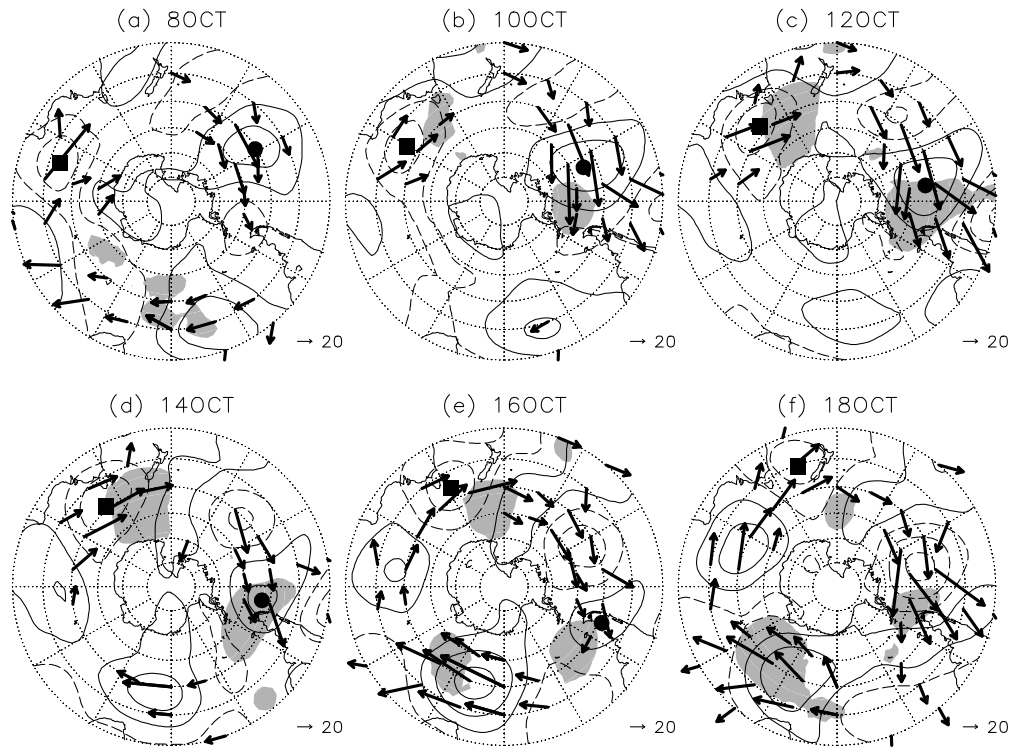


Figure 2. Maps of low-pass-filtered geopotential height anomalies (contoured: ± 50 , ± 150 and ± 250 m) and the horizontal component of an associated wave-activity flux (arrow) at the 400-hPa level, from 8 to 18 October, 1997 as indicated. Solid and dashed lines represent anticyclonic (positive) anomalies and cyclonic (negative) anomalies, respectively. Scaling for the arrows is given at the lower-right corner of each panel [Unit: m^2s^{-2}]. Shading indicates the upward component of the wave-activity flux exceeding $0.02 \text{ m}^2\text{s}^{-2}$ at the 150-hPa level. A closed circle and square indicate the tropospheric anticyclonic and cyclonic anomaly centres, respectively, as referred to in the text.

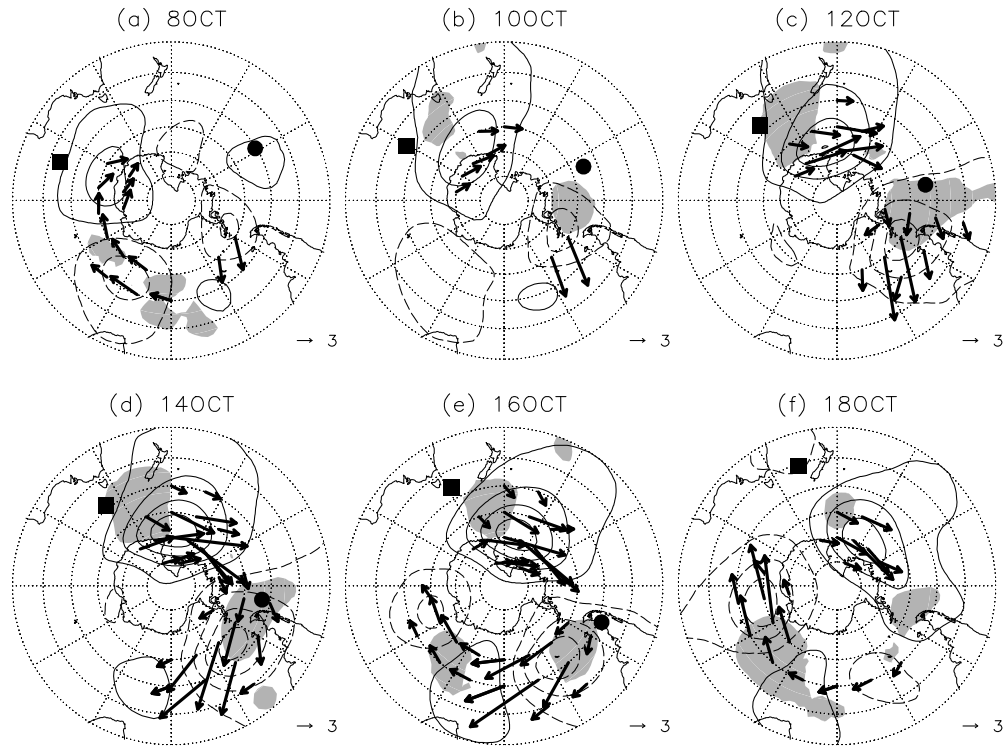


Figure 3. As in Fig. 2, but for low-pass-filtered 50-hPa geopotential height anomalies (contour: ± 60 , ± 180 , ± 300 and ± 420 m), and the horizontal component of the associated wave-activity flux (arrow). Shading indicates the upward component of the flux exceeding $0.02 \text{ m}^2\text{s}^{-2}$ at the 150-hPa level. A circle and square denote the same centres of the 400-hPa height anomalies as indicated in Fig. 2.

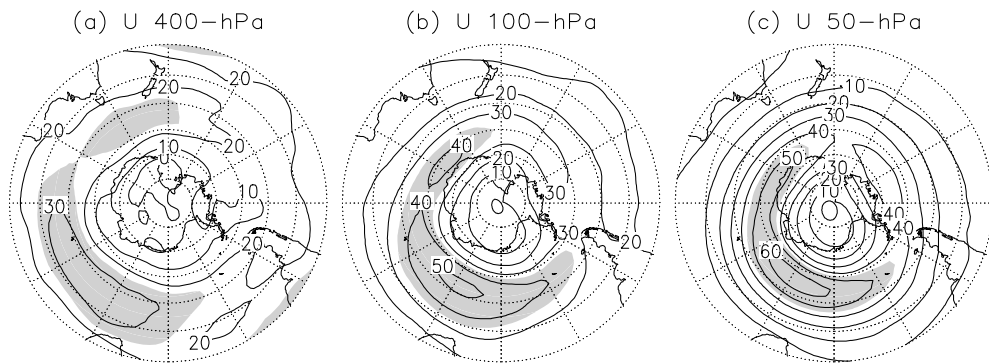


Figure 4. Mean westerly wind speed (U ; every 10 ms^{-1}) during the 31-day period centred at October 12 for the (a) 400-hPa, (b) 100-hPa and (c) 50-hPa levels. Shading: (a) $U \geq 25 \text{ [ms}^{-1}\text{]}$, (b) $U \geq 35 \text{ [ms}^{-1}\text{]}$, (c) $U \geq 45 \text{ [ms}^{-1}\text{]}$. Plotted poleward of 30°S .

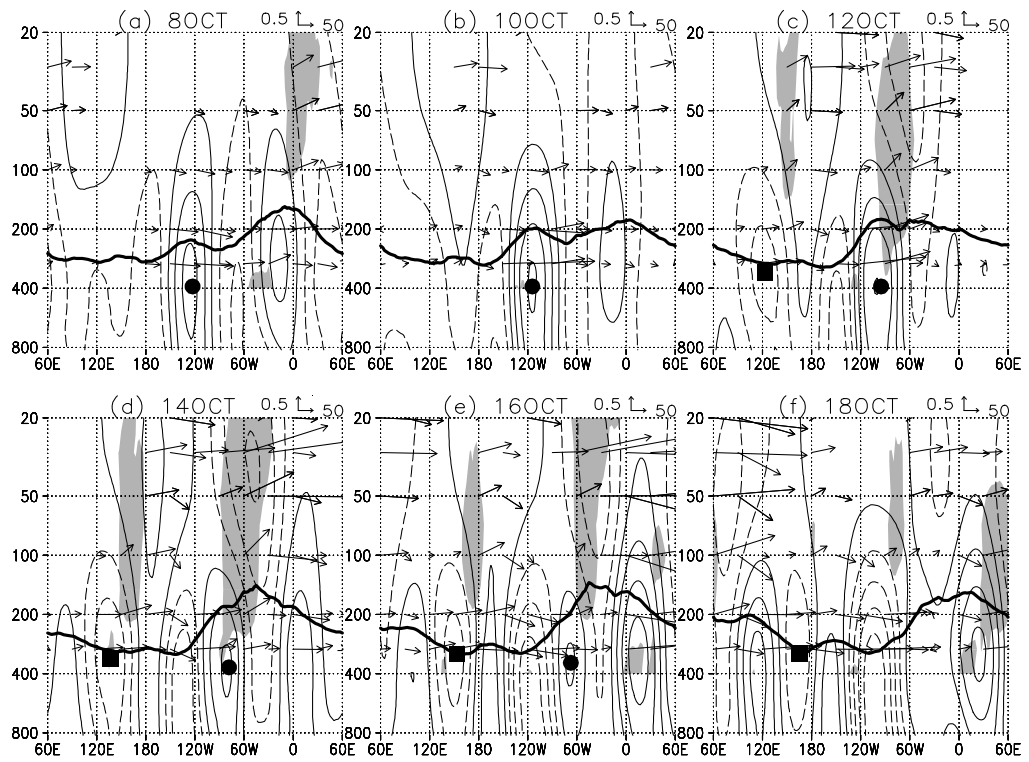


Figure 5. Zonal-height sections for 55°S of low-pass-filtered geopotential height anomalies (contour: ± 30 , ± 90 , ± 150 and ± 210 m) and the associated wave-activity flux (arrows), from 8 to 18 October, 1997 as indicated. Scaling for the arrows is given near the upper-right corner of each panel [Unit: m^2s^{-2}]. Solid lines represent anticyclonic (positive) anomalies and dashed lines cyclonic (negative) anomalies. Shading indicates the upward component of the flux exceeding $0.2 [\text{m}^2\text{s}^{-2}]$. The anomalies and flux have been normalized with pressure. A heavy line indicates the tropopause as defined by the NCEP. In each of the panels, a circle and square denote the centres of the tropospheric ψ' anomalies in the zonal section that correspond to the 400 hPa anticyclonic and cyclonic centres, respectively.

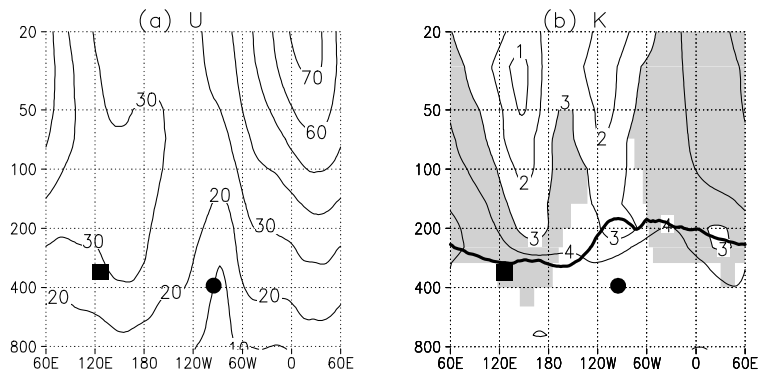


Figure 6. Zonal-height sections for 55°S of (a) zonal wind (U ; every 10 ms^{-1} ; shaded for $U \geq 25 \text{ ms}^{-1}$) and (b) refractive index (κ_s) of stationary Rossby waves, both based on the mean circulation in the 31-day period centered at 12 October, 1997. κ_s is represented as the equivalent zonal wavenumber for this latitude circle. Shading in (b) indicates the regions where $\kappa_s \geq 3$ and $U \geq 25 \text{ [ms}^{-1}]$. A heavy line in (b) denotes the tropopause defined by the NCEP. A circle and square indicate the centres of the upper-tropospheric anticyclonic and cyclonic centres, respectively, on 12 August as shown in Fig. 5c.

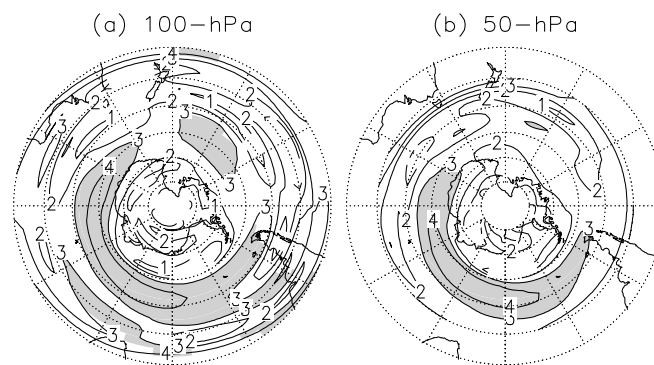


Figure 7. Maps of refractive index κ_s for stationary Rossby waves (represented as the equivalent zonal wavenumber for each latitude) at the (a) 100-hPa (b) and 50-hPa levels, both based on the mean circulation over the 31-day period centered at 12 October, 1997. Shading conventions are the same as in Fig. 6b.

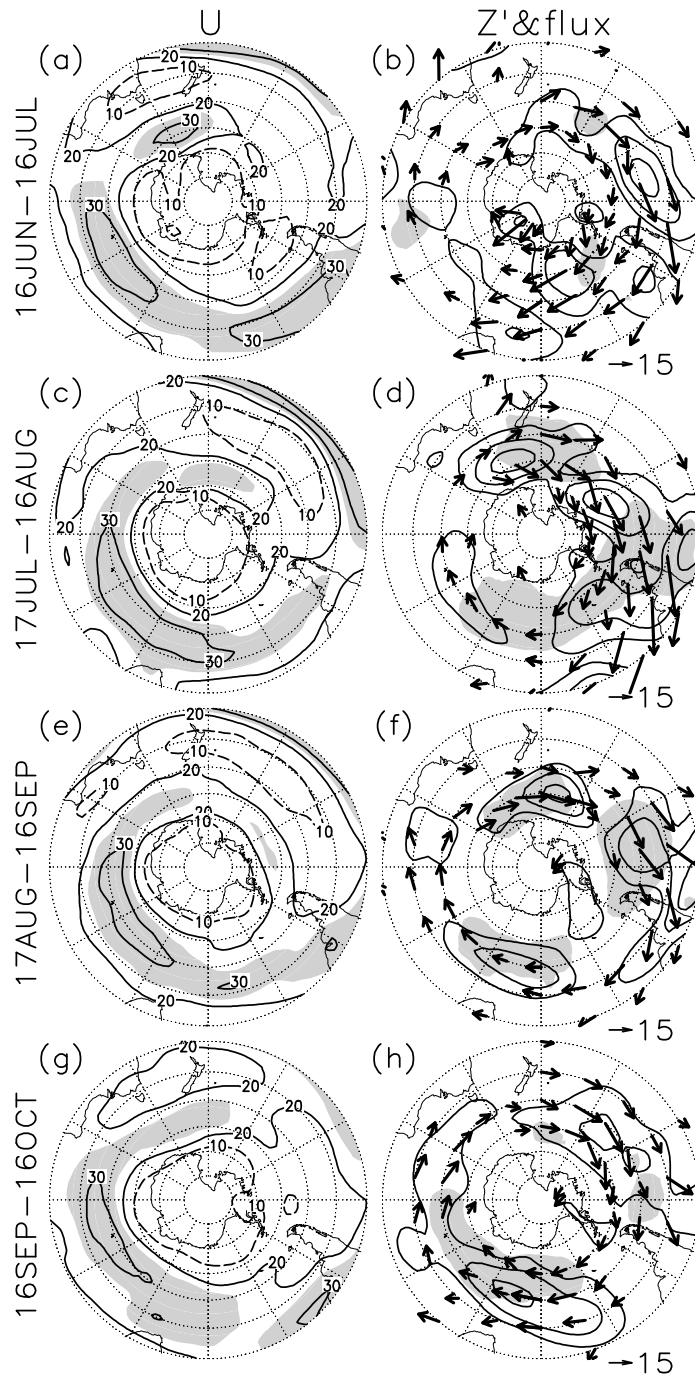


Figure 8. (a) Mean 400-hPa westerly wind speed (U : every 10 ms^{-1} ; dashed for $U=10 \text{ ms}^{-1}$; shaded for $U \geq 25 \text{ ms}^{-1}$) and (b) standard deviation of submonthly fluctuations $\sigma(\psi')$ in 400-hPa geopotential height (contoured for; 80, 110 and 140 m) superimposed on the horizontal component of a mean wave-activity flux (arrows), for Period I (16 June \sim 16 July, 1997). In (b), shading indicates the upward component of the mean wave-activity flux at the 150-hPa level exceeding $0.01 \text{ [m}^2\text{s}^{-2}\text{]}$. Scaling of the arrows (unit; m^2s^{-2}) is given near the lower-right corner of the panel. (c,d): Same as in (a,b), respectively, but for Period II (17 July \sim 16 August). (e,f): Same as in (a,b), respectively, but for Period III (17 August \sim 16 September). (g,h): Same as in (a,b), respectively, but for Period IV (16 September \sim 16 October).

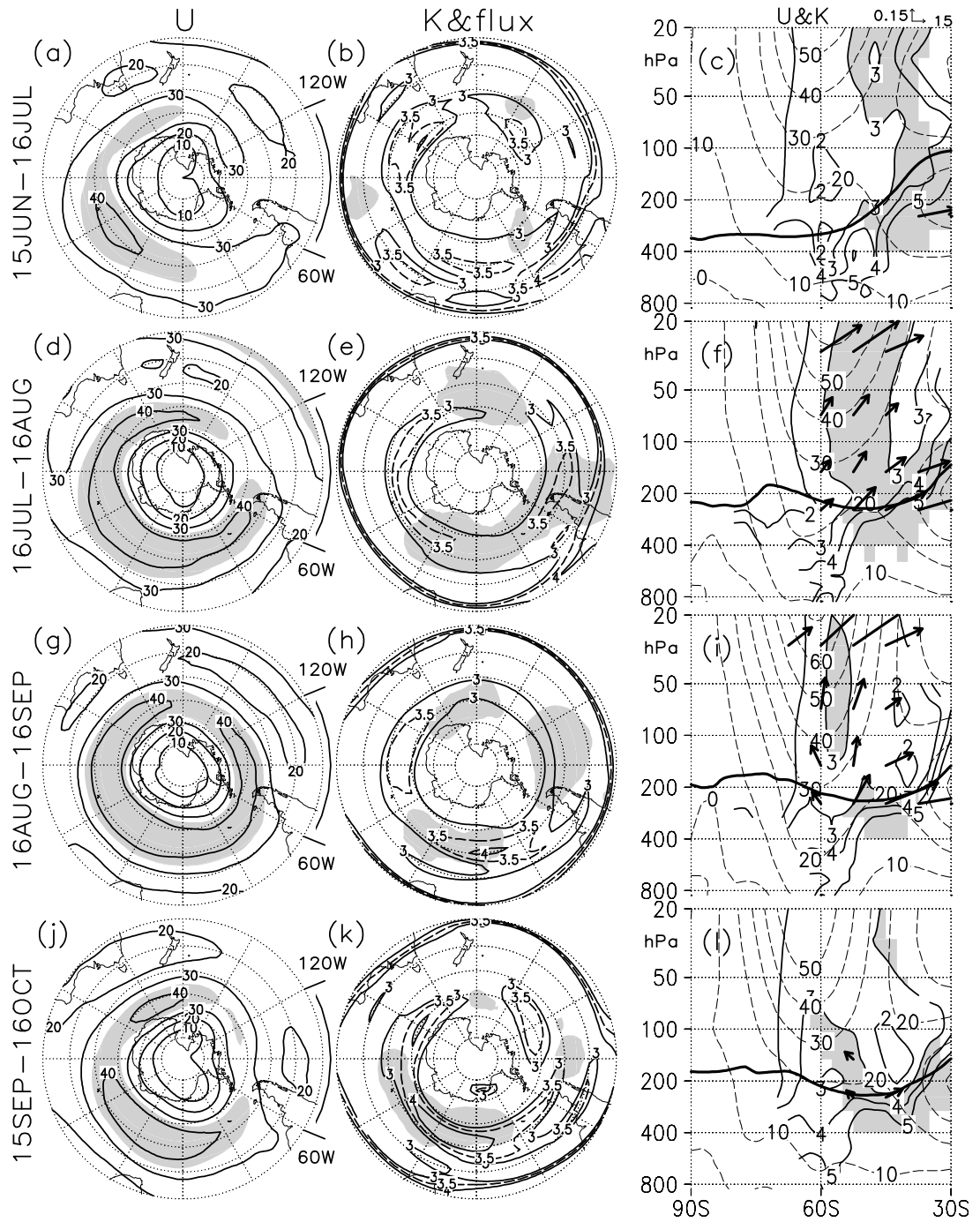


Figure 9. (a) Mean 100-hPa westerly wind speed (U : every 10 ms^{-1} ; shaded for $U \geq 35 \text{ ms}^{-1}$), (b) refractive index (κ_s) of stationary Rossby waves at the 100-hPa level, represented as the equivalent zonal wavenumber for each latitude, and (c) meridional section of κ_s (solid lines), U (dashed lines: every 10 ms^{-1}) and the meridional and vertical components of a mean wave-activity flux (arrows), all of which are averaged between 60°W and 120°W as indicated in (a), for Period I (16 June ~ 16 July, 1997). In (b), shading is applied where the upward component of mean wave-activity flux exceeds $0.01 \text{ [m}^2\text{s}^{-2}\text{]}$. In (c), shading indicates the regions for $\kappa_s \geq 3$ and $U \geq 25 \text{ [ms}^{-1}\text{]}$, and scaling for arrows is given at the right-upper corner of the panel. A thick line the tropopause defined by the NCEP. (d,e,f): Same as in (a,b,c), respectively, but for Period II (17 July ~ 16 August). (g,h,i): Same as in (a,b,c), respectively, but for Period III (17 August ~ 16 September). (j,k,l): Same as in (a,b,c), respectively, but for Period IV (16 September ~ 16 October).

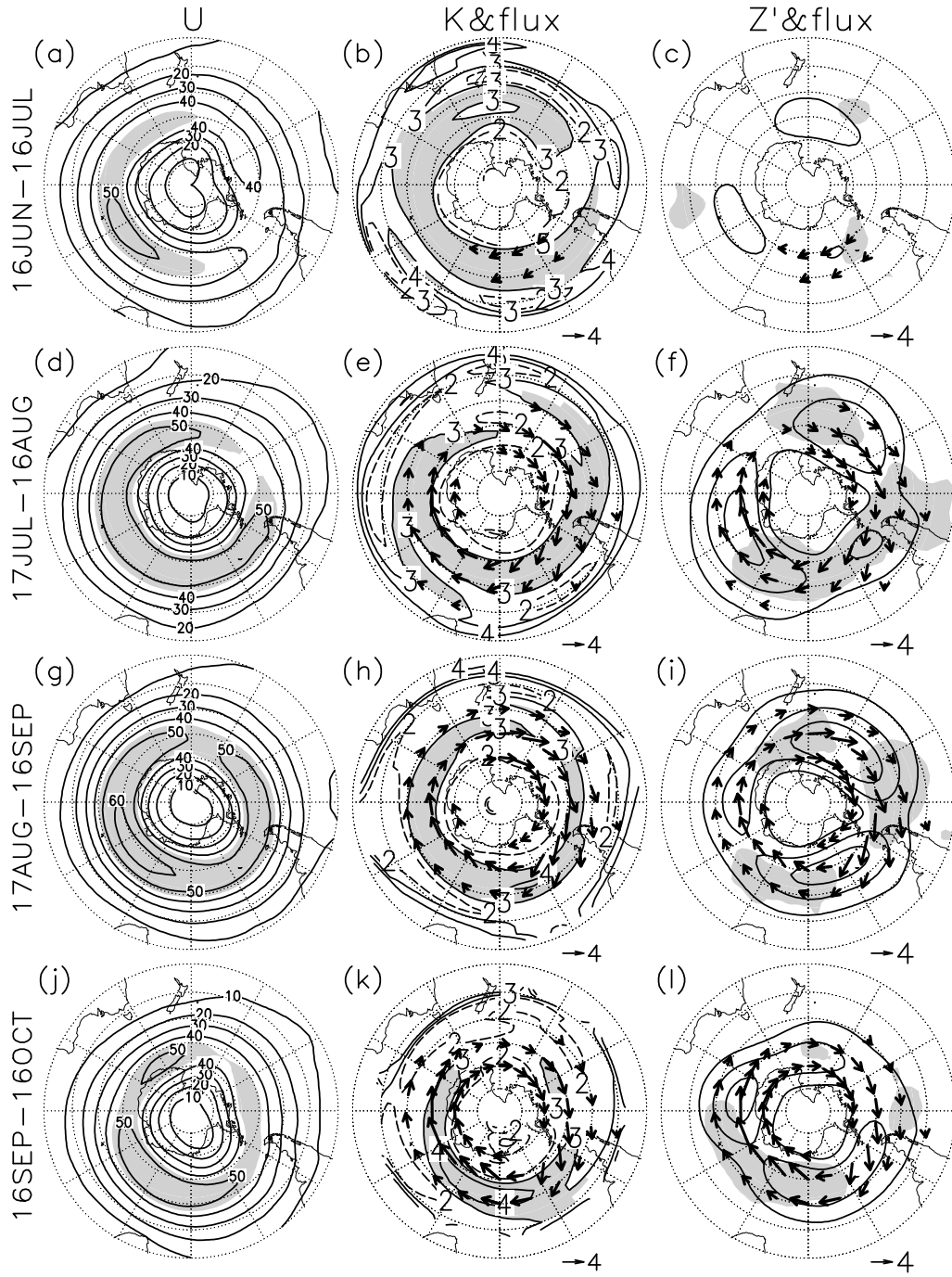


Figure 10. (a) Mean 50-hPa westerly wind speed (U : every 10 ms^{-1} ; shaded for $U \geq 45 \text{ ms}^{-1}$), (b) 50-hPa refractive index (κ_s) for stationary Rossby waves, represented as the equivalent zonal wavenumber for each latitude (contoured; dashed for $\kappa_s=2$) and the horizontal component of the mean wave-activity flux (arrows), and (c) standard deviation of submonthly fluctuations in 50-hPa geopotential height (contoured for 120, 200 and 280 m), and the horizontal component of the mean 50-hPa wave-activity flux (arrow), for Period I (16 June ~ 16 July, 1997). Scaling for arrows (unit; m^2s^{-2}) is indicated at the lower-right corner of each of (b) and (c). In (b), shading is applied where $\kappa_s \geq 3$ and $U \geq 45 \text{ [ms}^{-1}]$. In (c), shading is applied where the upward component of the 150-hPa mean wave-activity flux exceeds $0.01 \text{ [m}^2\text{s}^{-2}]$. (d,e,f): Same as in (a,b,c), respectively, but for Period II (17 July ~ 16 August). (g,h,i): Same as in (a,b,c), respectively, but for Period III (17 August ~ 16 September). (j,k,l): Same as in (a,b,c), respectively, but for Period IV (16 September ~ 16 October).

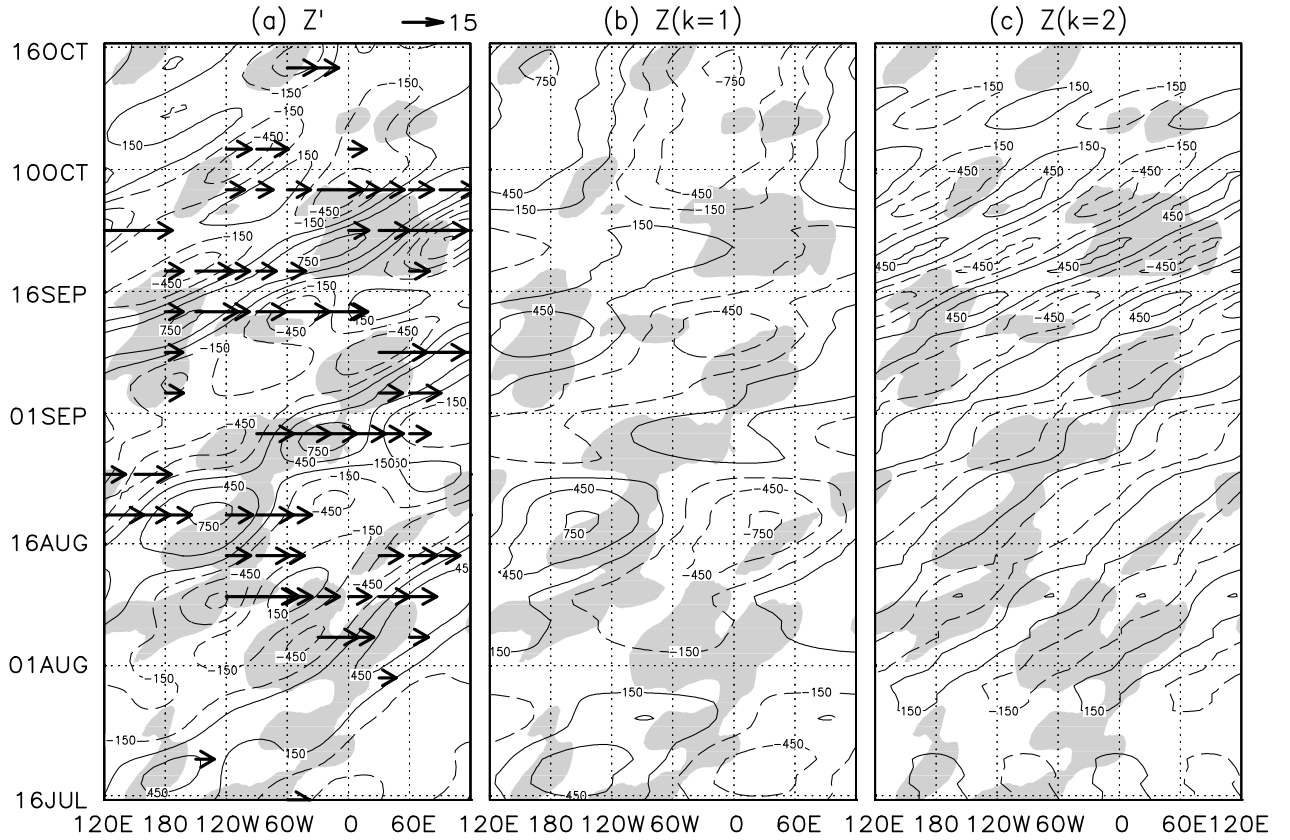


Figure 11. (a) Zonal-time section for our analysis period (16 July ~ 16 October, 1997) of 50-hPa geopotential height anomalies (contoured for ± 150 , ± 450 , ± 750 , ± 1050 and ± 1350 m) and the zonal component of a wave-activity flux (arrow), based on the meridional average between 55°S and 60°S . Solid and dashed lines indicate the positive and negative anomalies, respectively. Scaling for the arrows is given at the upper-right corner (unit: m^2s^{-2}). Shading indicates the upward component of the wave-activity flux exceeding $0.03 \text{ m}^2\text{s}^{-2}$ at the 150-hPa level. (b)-(c): As in (a), but for the (b) $k=1$ and (c) $k=2$ components, respectively, of planetary waves in the 50-hPa height field, including their climatological means.

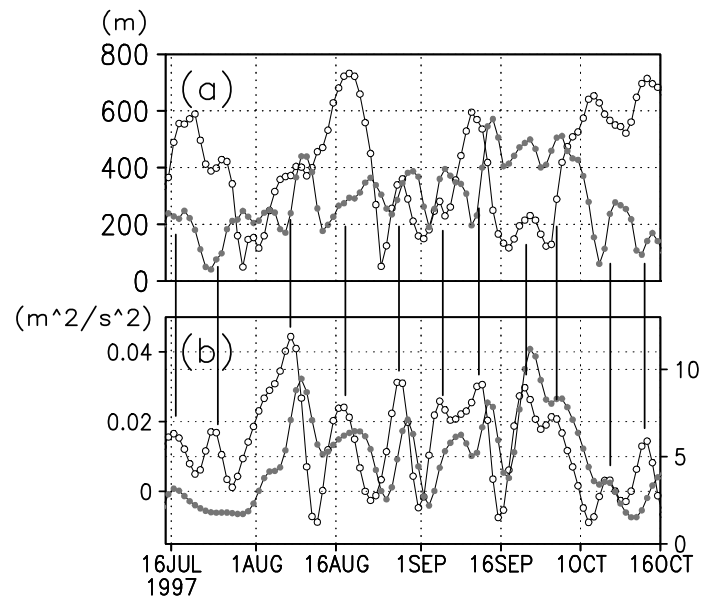


Figure 12. (a) Daily amplitudes (unit; m) of the $k=1$ (open circle) and $k=2$ (closed circle) components of 50-hPa planetary waves, both of which are meridionally averaged between 55°S and 60°S . (b) Daily time series of the vertical (150 hPa) and zonal (50 hPa) components of a zonal-mean wave-activity flux associated with the submonthly fluctuation (unit; m^2s^{-2}), averaged between 55°S and 60°S . Open circles signify the vertical component (left axis) and closed circles the zonal component (right axis).

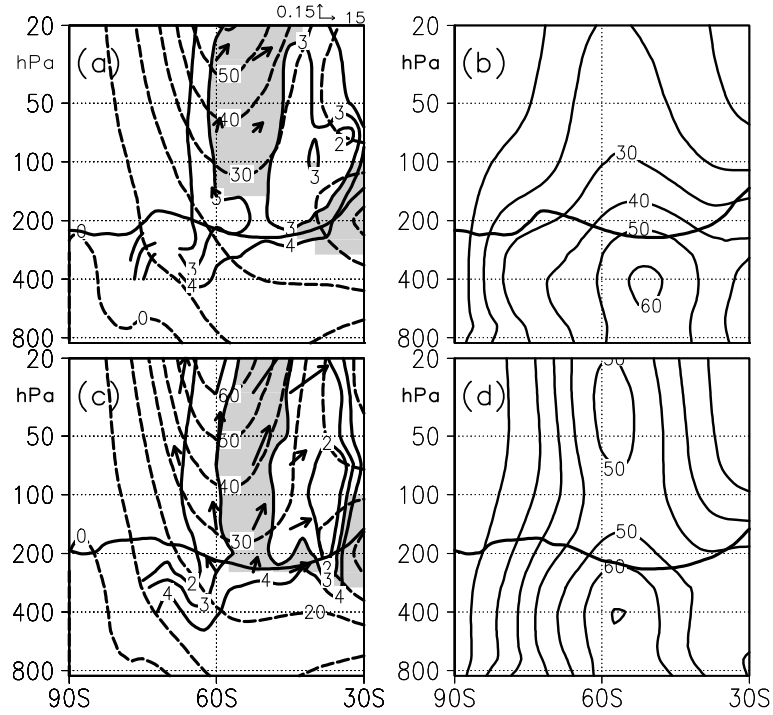


Figure 13. Meridional sections of (a) the zonal-mean U (dashed lines: every 10 ms^{-1}) and refractive index for stationary Rossby waves (κ_s) defined for the zonal-mean flow (solid line), superimposed on the E-P flux (arrow; scaling is at the right-upper corner; unit: m^2s^{-2}) for Period I. Shading indicates the regions for $\kappa_s \geq 3$ and $U \geq 35 \text{ [ms}^{-1}\text{]}$. A heavy line indicates the tropopause defined by the NCEP. (b) As in (a), but for the standard deviation of submonthly geopotential height fluctuations normalized by pressure (contoured for every 10 m). (c, d) As in (a) and (b), respectively, but for Period II.